Physics-Based Constitutive Model of Porous Materials for Die/Isostatic Compaction of Metallic Powders

Yujin Seong[1] · Dami Yim[1] · Min Ji Jang[1] · Jeong Min Park[1] · Seong Jin Park[2] · Hyoung Seop Kim[1]

Abstract

A physics-based constitutive model of porous materials is proposed to enhance the accuracy of numerical analysis in die/isostatic compaction. The correlation between the yield function and equivalent work equation was derived, and the numerical integration method was modified with the correlation. It is found that the apparent work of porous materials is lower than the product of relative density and equivalent work of solid materials at the beginning of compaction, implying the kinematic motion of powders and the resultant particle rearrangement. For verification of the proposed model, finite element analyses were performed for the die/isostatic compaction of three metal powders: Ti, SUS316L, and Al6061 powders. Compared with two conventional constitutive models, the proposed model improves the accuracy of the densification behaviors in all the stage during die/isostatic compaction. Furthermore, this study is a groundwork to link the densification behavior of porous materials at bulk scale to the particulate behavior of powders at microscale.

Keywords Constitutive model · Powder metallurgy · Die compaction · Porous material · Finite element method

1 Introduction

Powder metallurgy (PM) is widely used in the production of complex engineering parts due to the economic advantage of mass production in various industrial fields such as automobiles [1, 2], aerospace [3], and electronics. PM processing has three steps: pressing, sintering, and finishing. The mechanical properties of the final products processed by PM significantly depend on the deformation behavior of powders during these three steps. In particular, densification behavior of the powders during die-pressing is very important for the performance and reliability of the final product.

The numerical simulation of the powder compaction process is an alternative approach of experiments to investigate the densification behavior of powders due to efficiency and cost. The final aim of the numerical simulation is to control processing conditions, such as strain rate, pressure, and lubrication, and to optimize the mold design. Thus, it is important to use an appropriate constitutive model to correctly describe strain/stress distributions and density change of porous materials during the PM process.

Depending on the scale, there are two types of studies that develop constitutive models: phenomenological and micro-mechanics based approaches. In phenomenological studies, a powder bed is considered as continuous media, which is suitable for industrial applications. Meanwhile, micro-mechanics based approaches give us insight into the particulate behavior of the powder [4–10]. In their studies, a small representative volume element is employed to allow the particulate behavior to be taken in full account because each particle is simulated. Their final goal is to link the deformation behavior of porous materials at bulk scale to the particulate behavior at microscale.

Two phenomenological models are most commonly used in the PM field: The Green/Shima type model and the Drucker–Prager model. The Green/Shima type model [11–15] is a quadratic function of effective stress q and hydrostatic pressure p, as shown in Eq. (1),

$$A(R)q^2 + B(R)p^2 = \eta(R)Y_0^2 = Y_R^2, \qquad (1)$$

✉ Hyoung Seop Kim
   hskim@postech.ac.kr

[1] Department of Materials Science and Engineering, Pohang University of Science and Technology, Pohang 37673, Republic of Korea

[2] Department of Mechanical Engineering, Pohang University of Science and Technology, Pohang 37673, Republic of Korea

where $A(R)$, $B(R)$, and $\eta(R)$ are functions of relative density R. Y_0 is the yield strength of non-porous material and Y_R the yield strength of porous material. In the models, the yield strength of porous material is defined as the product of the yield strength of non-porous one and the strength ratio $\eta(R)$. This means that the deformation behavior of the non-porous one and the particle kinetics effect can be explained separately. Doraivelu et al. [13] revealed that $A(R)$ and $B(R)$ have a physical meaning, being associated with the apparent Poisson's ratio of porous materials. Despite the physical significance, the Green/Shima type model has limitations on compaction of the powder mixture because it is inconvenient to obtain the yield strength of the bulk material.

Recently, The Drucker–Prager cap (DPC) model [16] has been widely used for the compaction of the powder mixture and failure prediction of compacts with multiaxial stress analyses [17–21]. The DPC model originally was developed for soil/rock mechanics to predict the compressive failure of a wide range of brittle materials and the compressive inelastic deformation. This model can explain a strong link between the micromechanics of failure process and the macroscopic behavior. Due to the nature of soil/rock mechanics, however, it is difficult to give a physical meaning of each calibration parameter associated with the deformation behavior of porous materials.

Several researchers demonstrated that the shape of the yield surface depends on the loading history as well as relative density [22–24]. Cocks and Sinka [19, 20] developed a model which can consider loading history and relative density using the complementary work done per initial volume. It is worth mentioning two things. First, powders undergo large deformation with a very low yield stress at the early stage of compaction. Secondly, with the work of porous materials, the model can take into account both loading history and relative density.

On the other hand, the Green/Shima type model is implemented in the FEM by the numerical integration method developed by Aravas [25]. In their study, the equivalent plastic strain, one of the state variables, was determined with the equivalent work assumption, as follows:

$$\Psi = R\Psi_0. \tag{2}$$

That it, the apparent plastic work Ψ of porous material is equal to the product of relative density R and the equivalent plastic work of solid (i.e., non-porous) material Ψ_0. The above assumption is not appropriate considering the powder densification behavior at the early stage of compaction.

This paper proposes a new physics-based constitutive model of porous materials based on a yield function proposed by Kim [14, 15, 26] and an equivalent work assumption. A numerical integration algorithm is modified with the proposed model. We verified the improvement in the numerical accuracy by comparing the simulation and experimental results.

2 Theory: Correlations Between Yield Function and Equivalent Work Equation of Porous Materials

As proposed by Doraivelu et al. [13], a yield function is assumed that homogeneous and isotropic porous materials begin to yield when the apparent total deformation energy reaches a critical value. Up to yield point, density of porous materials is considered to be constant. This means spring back effect by elastic deformation can be neglected in this model.

The apparent stress σ_{ij} of porous materials is related to its deformation ε_{ij} by the following expression:

$$\sigma_{ij} = 2G^{app}\left(\varepsilon_{ij} - \frac{1}{3}\varepsilon_{ij}\delta_{ij}\right) + K^{app}\varepsilon^{vol}\delta_{ij}, \tag{3}$$

where G^{app} and K^{app} are the apparent shear and bulk modulus, respectively. ε^{vol} is a volumetric strain by the expression,

$$\varepsilon^{vol} = \varepsilon_{ij}\delta_{ij}. \tag{4}$$

The deviatoric strain can be rewritten from Eq. (3) so that

$$\varepsilon_{ij} - \frac{1}{3}\varepsilon^{vol}\delta_{ij} = \frac{1}{2G^{app}}\left(\sigma_{ij} - p\delta_{ij}\right), \tag{5}$$

where p is the hydrostatic pressure defined by

$$p = K^{app}\varepsilon^{vol} = \frac{1}{3}\sigma_{kk}. \tag{6}$$

The apparent work of porous materials Ψ is given by

$$\Psi = G^{app}\varepsilon^{dev2} + \frac{1}{2}K^{app}\varepsilon^{vol2}, \tag{7}$$

where $\varepsilon^{dev2} = \left(\varepsilon_{ij} - \frac{1}{3}\varepsilon^{vol}\delta_{ij}\right)\left(\varepsilon_{ij} - \frac{1}{3}\varepsilon^{vol}\delta_{ij}\right)$.

Equation (7) can be rewritten from Eq. 5 as follows:

$$\Psi = \frac{1}{4G^{app}}\left(\sigma_{ij} - p\delta_{ij}\right)\left(\sigma_{ij} - p\delta_{ij}\right) + \frac{1}{2K^{app}}p^2 = \frac{1}{6G^{app}}q^2 + \frac{1}{2K^{app}}p^2, \tag{8}$$

where $q^2 = \frac{3}{2}\left(\sigma_{ij} - p\delta_{ij}\right)\left(\sigma_{ij} - p\delta_{ij}\right)$, in which q is the effective stress of porous materials.

The equivalent work of solid materials is given by

$$\Psi_0 = G_0\varepsilon^{eq2} = \frac{1}{6G_0}Y_0^2. \tag{9}$$

Here, subscript 0 denotes solid materials. ε^{eq} and Y_0 are the equivalent strain and the associated yield stress, respectively.

In this work, the relationship between the apparent work of porous materials and that of solid is assumed as

$$\Psi = C(R)\Psi_0. \tag{10}$$

Here, $C(R)$ is assumed as a function of relative density. Substituting Eqs. (8) and (9) into Eq. (10), the following expression is obtained.

$$\frac{1}{6G^{app}}q^2 + \frac{1}{2K^{app}}p^2 = C(R)\frac{1}{6G_0}Y_0^2. \tag{11}$$

Since $K = \frac{2G(1+\nu)}{3(1-2\nu)}$, Eq. (11) can be expressed in the form,

$$\frac{2(1 + \nu^{app})}{3}q^2 + 3(1 - 2\nu^{app})p^2 = C(R)\frac{2(1 + \nu^{app})}{3}\frac{G^{app}}{G_0}Y_0^2, \tag{12}$$

where ν^{app} is the Poisson's ratio. Equation (12) follows the general form of a yield function of porous materials as shown in Eq. (1). In particular, the equation is the same as the yield function of Doraivelu et al. [13]. It is consistent with Martynova and Shtern [27] that the equivalent work is related with the yield function. $A(R)$ and $B(R)$ are given by

$$A(R) = \frac{2(1 + \nu^{app})}{3} = \frac{2 + R^2}{3}, B(R) = 3(1 - 2\nu^{app}) = 3\left(1 - R^2\right). \tag{13}$$

Here, $\nu^{app} = \nu_0 R^2$ is the relationship between Poisson's ratio and relative density suggested by Zhdanovich [28], and it was experimentally verified for aluminum and iron powders by Kuhn [29]. Assuming that the bulk material is incompressible, $\nu^{app} = \nu_0 = 0.5$. For bulk material, this yield function is the same as von Mises yield function.

Since Eq. (12) is equal to the yield function of porous materials [Eq. (1)], $\eta(R)$ is rewritten as

$$\eta(R) = C(R)\frac{2(1 + \nu^{app})}{3}\frac{G^{app}}{G_0}. \tag{14}$$

Kim [15] proposed the modified yield function considering the stress field of porous materials, where empirical function $\eta(R)$ is given by

$$\eta(R) = \left(\frac{R - R_c}{1 - R_c}\right)^n, \tag{15}$$

where R_c is the critical relative density below which the porous material has negligible strength. In general, R_c is the same as tap density of powders. n is the densification ratio. Koval'chenko [30] suggested the relationship between shear modulus and relative density for isotropic porous materials as follows:

$$G^{app}/G_0 = R^{m/R}. \tag{16}$$

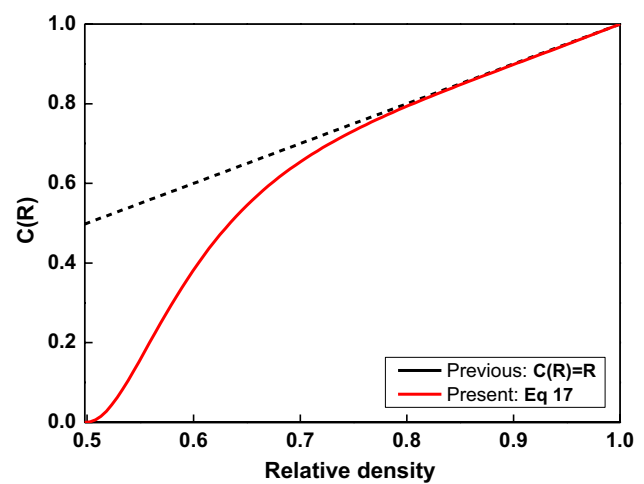Substituting Eqs. (15) and (16) into Eq. (14), $C(R)$ is obtained by

Fig. 1 Deformation energy ratio of porous and bulk materials $C(R)$

$$C(R) = \frac{3}{R^{m/R}\left(2 + R^2\right)}\left(\frac{R - R_c}{1 - R_c}\right)^n. \tag{17}$$

At the initial state, $C(R)$ is zero. As the relative density increases up to one (i.e., full density), $C(R)$ becomes one and, hence, the equivalent work equation becomes von Mises yield criterion.

What is the physical meaning of $C(R)$? Equation (2), generally used for porous material models, is suitable for describing porous materials including voids, but not for granular particles such as powders. Equations (10) and (17) are suggested for granular particles as well as porous materials. Figure 1 shows the modified model, Eq. (17) and the conventional model, $C(R) = R$. The modified model shows a significant difference from the conventional model as the relative density decreases. As the relative density increases, $C(R)$ approaches R. Consider the case where an external force is applied to the porous materials in each case. For voids, the applied force is converted to the deformation energy of the materials. For granular particles, however, the applied force is converted into the kinetic energy of the particles and the deformation energy of the materials so that the deformation energy of granular particles is reduced in comparison with the case with voids. As the relative density increases, granular particles become porous materials including voids.

3 Numerical Integration Method and Simulation Procedures

Aravas [25] developed a numerical integration method for pressure-dependent plasticity models, which is generally used for porous materials. In his study, the equivalent plastic strain is determined by the equivalent plastic work equation.

In the previous section, it was found that yield function is associated with equivalent work equation and $C(R)$ was derived as shown in Eq. (17). The necessary equations for the numerical integration are summarized as follows:

$$\Phi = A(R)q^2 + B(R)p^2 - \eta(R)Y_0^2 = 0, \tag{18}$$

$$\sigma_{ij} = p\delta_{ij} + \frac{2}{3}qn_{ij}, \tag{19}$$

$$\Delta\varepsilon_{ij}^p = \frac{1}{3}\Delta\varepsilon_p^{vol}\delta_{ij} + \Delta\varepsilon_p^{dev}n_{ij}, \tag{20}$$

$$\Delta H^1 = \Delta\varepsilon_p^{eq} = \frac{p\Delta\varepsilon_p^{vol} + q\Delta\varepsilon_p^{dev}}{C(R)Y_0}, \tag{21}$$

$$\Delta H^2 = \Delta R = -R\Delta\varepsilon_{vol}. \tag{22}$$

Here, Φ is a yield function and $n_{ij} = \partial q/\partial\sigma_{ij}$. The equivalent plastic strain ε_p^{eq} and relative density R are the state variables H^α, and their evolutions are described in Eqs. (21) and (22). The numerical integration method is modified according
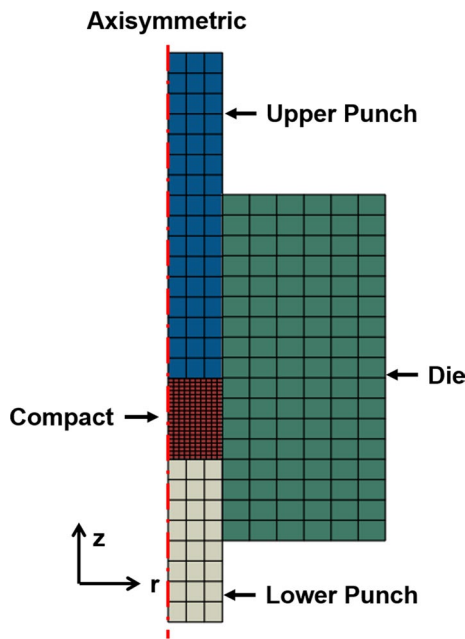
to these equations. The numerical integration derivation method is the same as that in references [25, 31, 32].

The FEM software ABAQUS (version 6.12) was employed for the implicit finite element analysis of the die compaction. The problem setup of the die compaction in this study is shown in Fig. 2. Coarse meshes were used for the molds, including upper/lower punches and die, because they deform elastically, and 480 four-node axisymmetric elements with reduced integration with hourglass control (CGAX4R) were used for the compact workpiece. An axisymmetric boundary condition in the centerline was applied to reduce the computational cost. External pressure was applied only to an upper punch with a fixed lower punch. A die could move freely along the axial direction. A penalty method with a friction coefficient of 0.2 was applied to describe mechanical interaction between the compact workpiece and molds. Heat generation by plastic deformation was ignored.

4 Materials and Model Parameter Calibration

The proposed model has four parameters: $A(R)$, $B(R)$, $C(R)$, and $\eta(R)$. These parameters are given in Eqs. (13), (15), and (17). In the equations, there are two coefficients which vary depending on the material: the densification rate n and the parameter related to the ratio of shear modulus, m.

In the study of Lee and Kim [14], the densification rate n was 2. The experimental data used in their study is shown in Fig. 3, which is the relationship between η and relative density. For iron, n is 2. For copper, two kinds of data are given depending on loading modes. In the study, n is fitted based on all data regardless of loading mode. When fitting each data, n values for tensile and compressive loading are 1.8
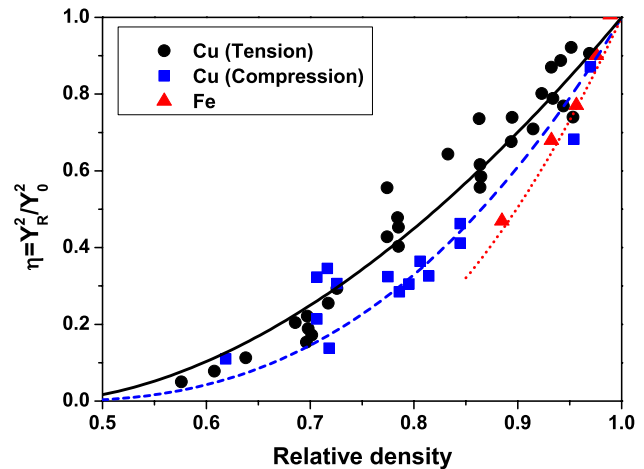
Fig. 2 Geometry and finite elements for die compaction

Fig. 3 Relationship between $\eta(R)$ and relative density. Experimental data on Cu [12] and Fe [33] is fitted to Eq. (15)

and 2.5, respectively. Loading mode during die compaction is compressive so that n is set to 2.5 for copper. From this point of view, n is a function of tap density, which is consistent with Ref. [15]. Figure 4 shows the relationship between n and tap density R_C, which is linearly fitted as follows:

$$n = -3.75R_c + 4.35. \qquad (23)$$

As mentioned in previous section, granular particles become porous materials including voids during densification. In the region where the relative density is large, the following equation must be satisfied.

$$\frac{\partial C}{\partial R} = C(R)\left\{ \frac{n}{R - R_0} - \frac{2R}{R^2 + 2} + \frac{m(lnR - 1)}{R^2} \right\} \leq 1. \qquad (24)$$

The parameter m takes the best-fit of Eq. (24), depending on n and tap density.

Three materials were chosen to verify the accuracy of the modified model: Titanium, SUS316L, and Al6061. For both SUS316L and Al6061, the experimental data were referred from Kwon et al. [34] and Lee and Kim [35], respectively. The experiments were carried out on Ti powders. Table 1 shows tap density and two calibrated parameters n, and m of three materials.
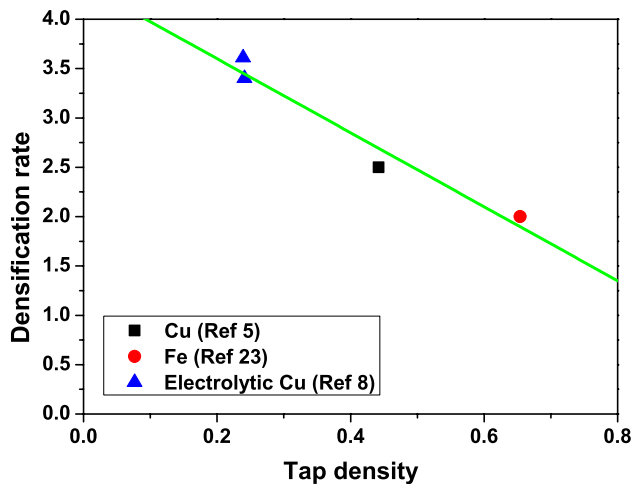
5 Experimental Procedures

Pure commercial Ti powder (grade 2) with an average particle size of 66.7 µm was used in the experiment. Figure 5a shows the powder morphology, which was analyzed using scanning electron microscopy (SEM). Figure 5b shows the particle size distribution determined using a laser particle size analyzer.

Ti powder with a weight of 4.24 g was poured into a die with a diameter of 10 mm. Zinc stearate was used as a die wall lubricant to minimize friction between the powders and molds. The compressive loading was applied to the upper punch, while the lower punch was fixed. The density of the green compact was measured by the Archimedes method using the Mettler Toledo XP205 instrument.

The hardness was also measured to obtain the density distribution of the compacts. For the measurement of the powder hardness, the cross-section parallel to the loading direction was mechanically polished with silicon carbide papers with 400, 600, 800, and 1200 grits and diamond suspensions of 3 and 1 µm. The hardness was measured using a micro Vickers hardness tester with a test load of 100 g and a retention time of 10 s. After the hardness measurement, the hardness values were translated into relative densities

Fig. 4 Relationship between densification rate and tap density

Table 1 Model parameters on modified Kim's model of various materials

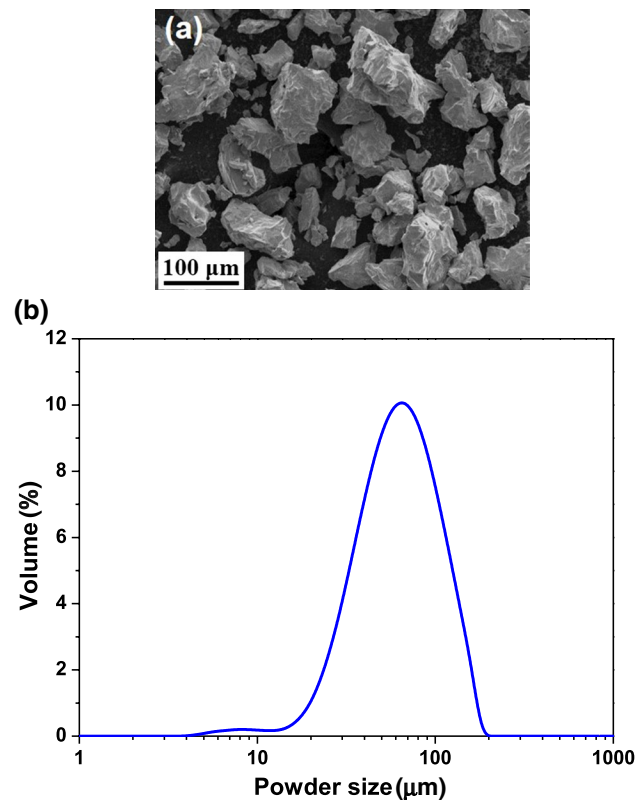| Material	Tap density	n	m
Ti (grade2)	0.4979	2.48	3.23
Al6061 (Ref 16)	0.5095	2.44	3.28
SUS316L (Ref 15)	0.64	1.95	3.75

Fig. 5 **a** Scanning electron micrograph and **b** distribution of particle size of Ti powder (grade 2)

using the relationship between relative density R and Vickers hardness Hv. The relationship is represented by the following equation:

$$R = \left(2.2 \times 10^{-3}\right)Hv + 0.4348. \tag{25}$$

Quasi-static compression tests on bulk materials were also performed at a strain rate of 10^{-3} s^{-1} using a universal testing machine (Instron 1361, USA). The digital image correlation (DIC) technique with an optical 3D deformation analysis system (ARAMIS 5 M, GOM Co., Germany) was used to measure precise strains. All specimens were finely polished using silicon carbide papers (300–1200 grits) and MoS2 spray was used as a lubricant to ensure proper conditions for uniaxial deformation and minimize friction effects. All the tests were performed at room temperature and were repeated at least three times at each strain rate to ensure the accuracy of the experimental data.

6 Results and Discussion

Figure 6 shows the uniaxial stress-plastic strain response of bulk Ti (grade 2) under compressive loading. The Kocks–Mecking–Estrin (KME) model [36, 37] was used for curve fitting, which represents the yield stress of bulk materials. This model is based on the well-known notion that the yield stress Y_0 is proportional to the square root of the dislocation density Z and proportional to the power law of the equivalent plastic strain rate $\dot{\varepsilon}_{eq}$,

$$Y_0 = Y_i \left(\frac{\dot{\varepsilon}_{eq}}{\dot{\varepsilon}_*}\right)^{1/m} \sqrt{Z}, \tag{26}$$

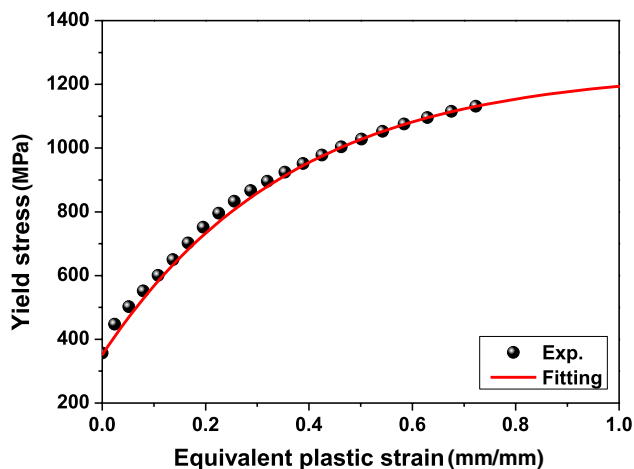where Z is the dislocation density normalized by its initial value, $\dot{\varepsilon}_*$ is the reference strain rate, m is a rate sensitivity parameter, and Y_i is the initial yield stress associated with the initial dislocation density.

The evolution of the normalized dislocation density Z involving both dislocation storage and annihilation is expressed as follows:

$$\frac{dZ}{d\varepsilon_{eq}} = c + c_1 \sqrt{Z} + c_2 Z, \tag{27}$$

where the constant c_1 and $c_2 = c_{20}\left(\dot{\varepsilon}_{eq}/\dot{\varepsilon}_0\right)^{-1/n}$ are associated with dislocation storage and dislocation annihilation by recovery, respectively. The parameter c_{20} is a proportionality constant, and n and $\dot{\varepsilon}_0$ are temperature dependent constants. The constant c is given by

$$c = M\frac{b}{d}\left(\frac{M\alpha G}{Y_i}\right)^2, \tag{28}$$

where M is the Taylor factor reflecting the texture, d is the grain size (or dislocation mean free path), b the magnitude of the Burgers vector, α is a numerical constant, and G is the shear modulus. The parameters for the yield stress were identified using the genetic algorithm from the experimental data as shown in Table 2. The elastic modulus is 110 GPa, and the elastic Poisson's ratio is 0.37.

Figure 7 shows the evolution of relative density during die compaction (Fig. 7a–c) and isostatic compaction (Fig. 7d) of various materials. Three models were used in the FEM simulations: Kim (previous), modified Kim (present), and Shima–Oyane models. The associated model parameters are summarized in Table 3. The modified Kim's model improves the accuracy of the simulation compared to Kim's model. Kim's model sometimes overestimates the relative density as shown in Fig. 7a, b. Because the difference between the two models is only $C(R)$, it implies that the equivalent plastic strain is underestimated for previous model. For Al6061 powders, the difference in relative density between two models is negligible in the case of die (Fig. 7c) and isostatic compaction (Fig. 7d). The modified one predicts more accurately the relative density than the Shima–Oyane one at the beginning of the compaction.

Fig. 6 Stress–plastic strain relationship for bulk Ti (grade2)

Table 2 Parameters for the yield stress of Ti (grade 2)

Parameter	Value	Parameter	Value
M	3.1	b	0.295 nm
d	120 μm	α	0.3
c_1	19.76	c_{20}	5.03
n	50	m	30.52
Y_i	349.63 MPa	$\dot{\varepsilon}_{eq}$	0.0055 s^{-1}
$\dot{\varepsilon}_0$	1 s^{-1}	$\dot{\varepsilon}_*$	0.005 s^{-1}
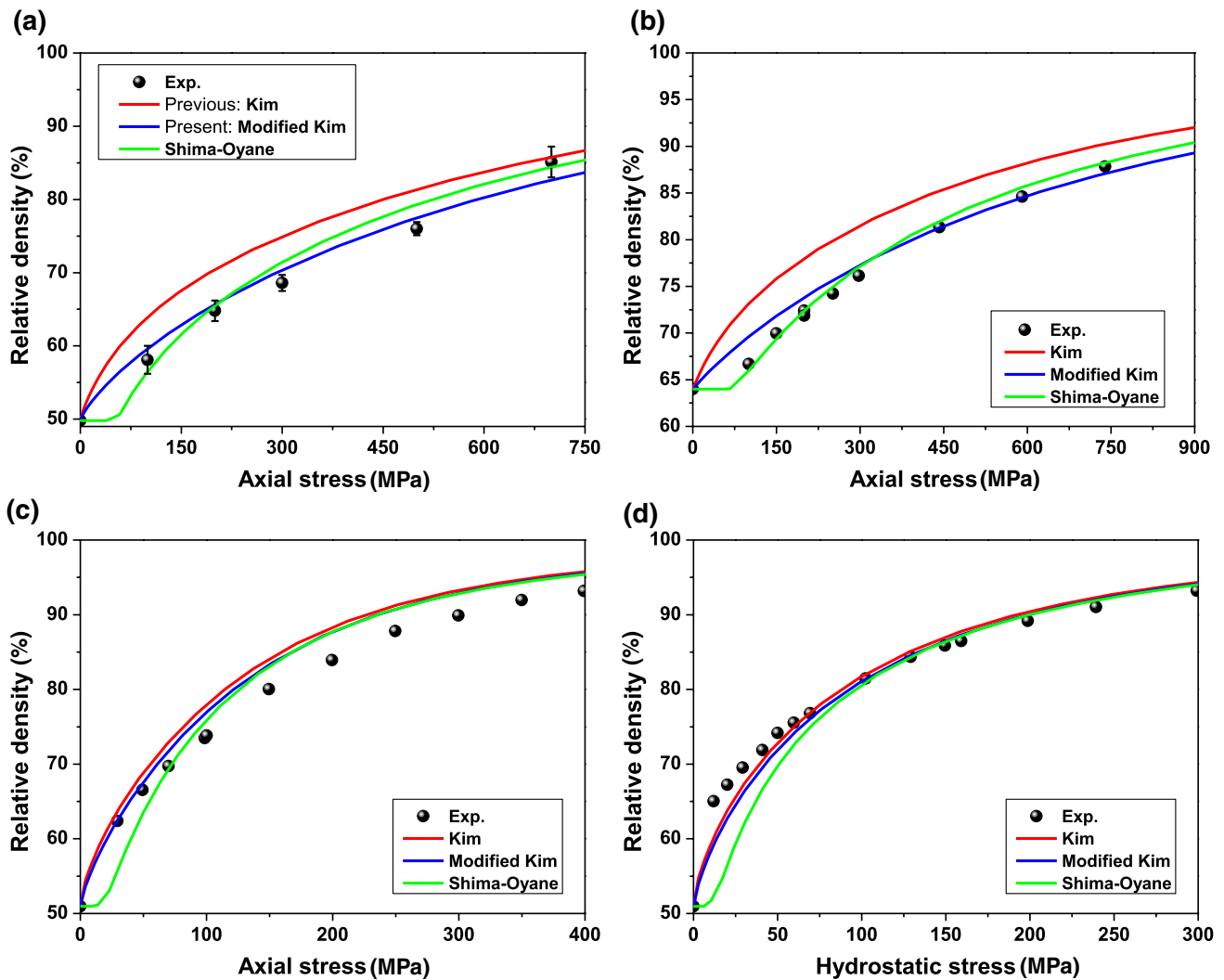
Fig. 7 Evolution of relative density during die compaction of **a** Ti, **b** 316L stainless steel, and **c** Al6061 powder and during isostatic compaction of **d** Al6061 powder

Table 3 Model parameters on yield criterion [Eq. (1)] and the equivalent work equation [Eq. (10)]

	$A(R)$	$B(R)$	$\eta(R)$	$C(R)$
Modified Kim (present)	$\frac{2+R^2}{3}$	$3\left(1-R^2\right)$	$\left(\frac{R-R_c}{1-R_c}\right)^n$	Equation 17
Kim [8]	$\frac{2+R^2}{3}$	$3\left(1-R^2\right)$	$\left(\frac{R-R_c}{1-R_c}\right)^n$	R
Shima-Oyane [5]	$\frac{1}{1+0.6889(1-R)^{1.028}}$	$\frac{9\times0.6889(1-R)^{1.028}}{1+0.6889(1-R)^{1.028}}$	$\frac{R^5}{1+0.6889(1-R)^{1.028}}$	R

Figure 8 shows the changes in equivalent plastic strain and yield stress of the porous materials Y_R to relative density. In the modified model, the equivalent plastic strain drastically increases at the beginning of compaction (Fig. 8a), whereas the yield stress sharply increases for the Shima–Oyane one (Fig. 8b). It is worth noting the physical meaning. There are randomly distributed powders in the early stage of compaction. The powders move and rearrange when compressive loading is applied, implying that the increase in apparent plastic strain of materials is more reasonable.
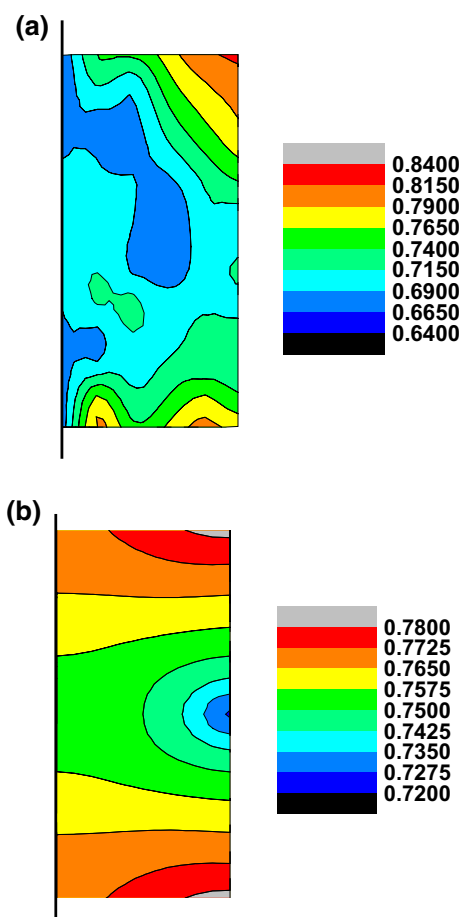
Figure 9 shows the relative density distribution of the experimental and simulation results under the axial stress of 500 MPa. The experimental distribution was obtained using Eq. (25). The distribution of the simulation results was obtained with a friction coefficient of 0.2 between the

(a)

(b)
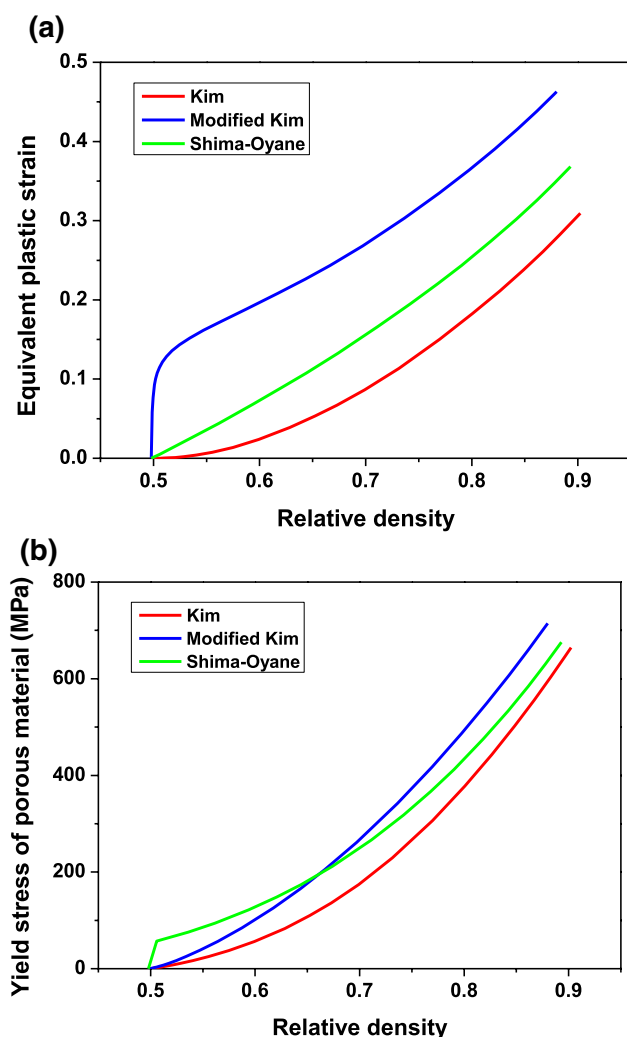
Fig. 8 Change of **a** equivalent plastic strain and **b** yield stress of porous material to relative density during die compaction of Ti powder

(a)

(b)

Fig. 9 Relative density distribution of **a** experimental data and **b** simulation result of Ti powder compact pressed of 500 MPa

powder and mold. The density is the lowest near the mid-surface of the compact and the highest at both ends. This is because the die can move freely along the axial direction. The relative density distribution of the simulation results has a tendency similar to that of the experimental ones. The qualitative agreement is good; however, the quantitative agreement of the relative density is not perfect because of several sources, such as experimental imperfections and numerical artifacts. Indeed, we performed the powder compaction using hand type press rather than hydraulic machine equipment. In this compaction process, there can be influence of shaft misalignment and vibration of the hand press and die.

Summarizing the advantages and limitations of the proposed model, there are three advantages. First, this model can separately explain the mechanical properties of non-porous material and the effect of powder morphology.

Therefore, when the stress–strain relationship of a non-porous material and tap density of powders are known, the densification behavior of the powders can be predicted using this model. Secondly, this model can give the physical meaning of three terms related to micromechanics: strength ratio η and two apparent mechanical properties v^{app} and G^{app}. Finally, this model does not depend on the powder shape unlike the work of Cocks and Sinka [19, 20]. In their work, the complementary work of porous material was obtained assuming a spherical powder shape. However, as explained in Sinka and Cocks' reports, the proposed model based on the work done per current volume could be degraded if other modes of force are applied instead of die/isostatic compaction.

7 Summary

A physically-based constitutive model of porous materials was proposed to enhance the accuracy of numerical analysis in die/isostatic compaction. The correlation between the

yield function and the equivalent work equation was derived, and the numerical integration method was modified with the correlation. It is found that the apparent work of porous materials is lower than multiplication of relative density and equivalent work of solid materials at the beginning of compaction, implying kinematic motion of powders and the resulted particle rearrangement. Finite element analyses (FEA) were performed for die/isostatic compaction of three metal powders. Compared with two constitutive models, the proposed model improves the accuracy of the densification behavior in all the stage during die/isostatic compaction. With this model, the deformation of porous materials can be easily predicted using tap density and stress-strain relationship of a solid material, because two model parameters n and m have dependency on tap density. The proposed model predicts the final green density well, given the compressive loading exerted on the powders. Furthermore, this model can give the physical meaning of three terms related to micromechanics: strength ratio η, and two apparent mechanical properties v^{app}, and G^{app}. This study could provide a link between micromechanics and phenomenological models for powder densification behavior.

References

1. B.D. Soane, P.S. Blackwell, J.W. Dickson, D.J. Painter, Soil Tillage Res. **1**, 373 (1980/1981)
2. T. Saito, JOM **56**, 33 (2004)
3. J.R. Pickens, J. Mater. Sci. **16**, 1437 (1981)
4. C.L. Martin, D. Bouvard, G. Delette, J. Am. Ceram. Soc. **89**, 3379 (2006)
5. P. Pizette, C.L. Martin, G. Delette, P. Sornay, F. Sans, Powder Technol. **198**, 240 (2010)
6. B. Harthong, J.-F. Jerier, P. Doremus, D. Imbault, F.-V. Donze, Int. J. Solids Struct. **46**, 3357 (2009)
7. B. Harthong, J.-F. Jerier, V. Richefeu, B. Chareyre, P. Doremus, D. Imbault, F.-V. Donze, Int. J. Mech. Sci. **61**, 32 (2012)
8. A. Salvadori, S. Lee, A. Gillman, K. Matous, C. Shuck, A. Mukasyan, M.T. Beason, I.E. Gunduz, S.F. Son, Mech. Mater. **112**, 56 (2017)
9. Y. Huang, J. Li, Y. Teng, X. Dong, X. Wang, G. Kong, T. Song, Powder Technol. **320**, 668 (2017)
10. L. Kempton, D. Pinson, S. Chew, P. Zulli, A. Yu, Powder Technol. **320**, 586 (2017)
11. H.A. Kuhn, C.L. Downey, Int. J. Powder Metall. **7**(1), 15 (1971)
12. S. Shima, M. Oyane, Int. J. Mech. Sci. **18**, 285 (1976)
13. S.M. Doraivelu, H.L. Gegel, J.S. Gunasekera, J.C. Malas, J.T. Morgan, J.F. Thomas, Int. J. Mech. Sci. **26**(9/10), 527 (1984)
14. D.N. Lee, H.S. Kim, Powder Metall. **35**, 275 (1992)
15. H.S. Kim, Meter. Sci. Eng. A **251**, 100 (1998)
16. D.C. Drucker, W. Prager, Q. Appl. Math. **10**, 157 (1952)
17. J. Almanstotter, Int. J. Refract. Met. Hard Mater. **50**, 290 (2015)
18. M. Zhou, S. Huang, J. Hu, Y. Lei, Y. Xiao, B. Li, S. Yan, F. Zou, Powder Technol. **305**, 183 (2017)
19. A.C.F. Cocks, I.C. Sinka, Mech. Mater. **39**, 392 (2007)
20. I.C. Sinka, A.C.F. Cocks, Mech. Mater. **39**, 404 (2007)
21. H. Diarra, V. Mazel, V. Busignies, P. Tchoreloff, Powder Technol. **320**, 530 (2017)
22. N.A. Fleck, J. Mech. Phys. Solids **43**, 1409 (1995)
23. A.R. Akisanya, A.C.F. Cocks, N.A. Fleck, Int. J. Mech. Sci. **39**, 1315 (1997)
24. I. Sridhar, N.A. Fleck, Acta Mater. **48**, 3341 (2000)
25. N. Aravas, Int. J. Numer. Methods Eng. **24**, 1395 (1987)
26. H.S. Kim, Y. Estrin, E.Y. Gutmanas, C.K. Rhee, Mater. Sci. Eng. A **307**, 67 (2001)
27. I.F. Martynova, M.S. Shtern, Soviet Powder Metall. Met. Ceram. **17**, 17 (1978)
28. G.M. Zhdanovich, *Theory of Compacting of Metal Powders* (Foreign Technology Division Wright-Patterson Air Force Base, Dayton, 1971)
29. H.A. Kuhn, in *Powder Metallurgy Processing: The Techniques and Analyses*, ed. by H.A. Kuhn, A. Lawley (Acadamic Press, New York, 1978), p. 99
30. M.S. Koval'chenko, Powder Metall. Metal Ceram. **32**(3), 268 (1993)
31. Z.L. Zhang, Comput. Methods Appl. Mech. Eng. **121**, 29 (1995)
32. Z.L. Zhang, Comput. Methods Appl. Mech. Eng. **121**, 15 (1995)
33. S.B. Biner, W.A. Spitzig, Acta Metall. Mater. **38**(4), 603 (1990)
34. Y.S. Kwon, H.T. Lee, K.T. Kim, J. Eng. Mater. Technol. **119**, 366 (1997)
35. S.C. Lee, K.T. Kim, Int. J. Mech. Sci. **44**, 1295 (2002)
36. H. Mecking, U.F. Kocks, Acta Matall. **29**, 1865 (1981)
37. Y. Estrin, in *Unified Constitutive Laws of Plastic Deformation*, ed. by A.S. Krausz, K. Krausz (Academic Press, San Diego, 1996), p. 69

Publisher's Note Springer Nature remains neutral with regard to jurisdictional claims in published maps and institutional affiliations.